3D PRINTING OF CEMENTITIOUS MATERIALS WITH SUPERABSORBENT POLYMERS: A DURABLE SOLUTION?

J. Van Der Putten (1)*, D. Snoeck (1), G. De Schutter (1) and K. Van Tittelboom (1)*

(1) Magnel Laboratory for Concrete Research, Ghent University, Tech Lane Ghent Science park, Campus A, Technologiepark-Zwijnaarde 60, 9052, Ghent, Belgium

* Corresponding author: Kim.VanTittelboom@UGent.be

Abstract

Nowadays, 3D printing of cementitious materials is a hot research topic in the construction industry. This construction method is capable of producing complex geometries and large-scale components without the use of expensive formwork. However, due to the lack of molding, more shrinkage will be induced and the amount of cracks will increase. As this phenomenon introduces ingress paths for chemical substances, it will affect the durability of the printed element in a negative way. One potential way to tackle this disadvantage is to include superabsorbent polymers (SAPs) in the cementitious material. As these polymers are able to absorb part of the mixing water and to release it during hardening, they induce internal curing and can mitigate self-desiccation and autogenous shrinkage. Another positive effect of using SAPs is the increased moisture content of the printed surface, enhancing the bond between two subsequent layers. For the aim of this research, two different SAPs were used to fabricate printed elements and the microstructural changes are correlated with their influence on durability and sustainability. First results showed that in general, the addition of superabsorbent polymers decreases the shrinkage in printed materials. They also reduce the nanoporosity in the range of 100 nm to 500 nm and increase the amount of voids with a diameter above 700 nm, resulting in less microcracks and a decreased amount of preferential ingress paths for chemical substances. On the other hand, the total air content increases with the addition of SAPs, proportional to the amount of SAPs added.

Keywords: 3D printing, hydrogels, shrinkage, microstructure

1. INTRODUCTION

3D printing is an innovative way of building with ‘traditional’ concrete. The utmost advantage of this technique – one of the main reasons that it exists, in fact – is the absence of costly formwork. This formwork usually requires a lot of manual labor, translated these days in a huge cost. The second main advantage is the freedom of form of the printed elements. The latter has a similar effect on the projects economy, as does the first: cost reduction [1, 2].

However, prior to revolution in the construction practice, there is a period of study and optimization. Concrete for printing needs to fulfill conflicting requirements. First, there is the

work- or printability that demands a good flow in the printer tubes and nozzle. This means that the material may not settle too fast in the reservoir and blocking in the tubing must be prevented. Second, an adequate buildability is necessary, requiring a material that is viscous enough. It should not set too fast in order to have a good bonding, and not too slow to obtain enough strength for support of the next layer. These demands do not solely depend on the cementitious characteristics but on the printing procedure as well. Time plays a leading role in this performance. Apart from the additional requirements set by the new technology, the concrete faces problems inherent to its mix design, indifferent to the procedure. Due to the lack of molding and the layered end result, shrinkage and void formation are the major issues that need to be counteracted. As both phenomena increase the risk for crack formation, they will affect the durability and mechanical performance of the printed element in a negative way.

In search of possible solutions, scientists have turned to superabsorbent polymers (SAPs) [3, 4]. As these polymers are able to absorb part of the mixing water and to release it during hardening, they induce internal curing and can mitigate self-desiccation and autogenous shrinkage. Another positive effect of using SAPs is the increased moisture content of the printed surface, enhancing the bond between two subsequent layers. In order to correlate the microstructural changes with their durable behavior, two types of SAPs with the same chemical composition but with slightly different size, were added to a reference mixture. The durability of the mixture was evaluated based on shrinkage measurements and correlated with the formation of voids and pores, measured with mercury intrusion porosimetry (MIP) and air void analysis.

2. MATERIALS AND METHODS

2.1. Materials and mix composition

The reference mixture contained an ordinary Portland Cement (CEM I 52.5 N Strong) combined with standard sand with a maximum particle size equal to 2 mm (0/2), water (W/C = 0.35) and a polycarboxylic ether (PCE) with a molecular weight of approximately 4000 g/mol and 35% solids to increase the flowability. An additional $(W/C)_a$ of 0.063 was added to the mixtures with SAPs, following the theory of Poders and Brownyard [5]. The amount of both superabsorbent polymers (type A and P) was obtained after evaluating the flow table test and equals respectively 0.17 and 0.15 mass% of cement weight. The composition of the mixtures with and without the addition of SAPs can be found in Table 1.

Table 1: Mix composition (with and without the addition of SAPs)

Mixture	CEM I 52.5N Strong [kg/m³]	Sand 0/2 [kg/m³]	Water [kg/m³]	SP [woc%]	SAP [moc%]
REF	620.5	1241	226.5	0.15	-
SAP A	620.5	1241	260.6	0.15	A = 0.17
SAP P	620.5	1241	260.6	0.15	P = 0.15

Both polymers have an irregular shape, are bulk-polymerized monovalent salt polyacrylate types and more detailed information can be found in Table 2 [3]. The below mentioned swelling times are measured in demineralised water and are the time needed for a SAP to reach maximal

saturation while being in a vortex. The absorption capacity was obtained through the filtration test after 24h in demineralized water [6].

Table 2: Specifications of the applied superabsorbent polymers (SAPs)

SAP	Type	Company	Size [µm]	Swelling time [sec]	Absorption Capacity [g/g]
A	Copolymer of acrylamide and sodium acrylate	BASF	100 ± 22	10	305 ± 4
P	Cross-linked potassium salt polyacrylate	Evonik Industries	190 ± 61	14	286 ± 1

2.2. 3D printing process

A custom-made apparatus was used to simulate an extrusion-based 3D printing process. The nozzle of the print equipment had an elliptical shape (28 mm x 18 mm) and was capable of printing layers with a maximum length of 300 mm. The height of the layers was manually adjustable. Within this research, two layered specimens were printed, where each layer height equaled 15 mm and the sample width was approximately 30 mm. The printing speed was kept constant at 1.7 cm/s. The effect of an increased interlayer time gap between the layers was not considered within the scope of this research.

2.3. Shrinkage

Shrinkage is one of the mayor obstacles for printed elements and as mentioned before, it will cause unwanted deformations. Especially when the deformations are restrained, for example after printing the second layer, shrinkage may lead to (tensile) stresses and cracking degrading the quality of the printed element. Due to the lack of moulding, mainly drying shrinkage plays an important role. As no standardised techniques are available for measuring the (early age) shrinkage of printed elements, new methods were devised.

An evaluation of the unrestrained shrinkage was based on six different measuring points, placed at the top of a printed layer directly after extrusion and positioning in between two cameras to measure the shrinkage in longitudinal direction. During the first 24h, the pictures were analysed with 20 images at a time every 5 minutes, with a digital mesh of 15 x 15 pixels applied to the surface of interest. The following 6 days, photographs were analysed at 30-minutes intervals, 30 images at a time and with the same pixel size implemented. The earliest photograph was taken as reference for all others, to which the mean technical strain ε_y [µm/mm] was calculated based on Eq. (1):

$$\varepsilon_y\,[\mu m/mm] = \left(\frac{\Delta l}{l_0}\right)_i \quad (1)$$

in which Δl [mm] equals the difference in length of the complete surface and l_0 [mm] is the initial length of the surface. Shrinkage measurements were performed for 168 hours in standardized circumstances (20±3°C, 60±5% RH) and the measurements were executed in triplicate for each mixture.

To exclude autogenous shrinkage from the overall shrinkage, corrugated tubes measurements were performed according to ASTM C1698. For these test, a polyethylene normative corrugated mould was filled and sealed afterwards. The tube was ensured to have an

end-to-end length of 420 mm. The exact initial length was measured manually and used to accurately obtain the lengths at later ages. Afterwards, the tube was placed in an automatic continuous measuring frame with digital dilatometers having a deformation range of 5 mm. Each mix design was observed in triplicate for 7 days, recording the movement every 10 minutes. The linear autogenous strain is obtained as follows (Eq. (2)).

$$\varepsilon_{auto}[\mu m/m] = \left(\frac{L(t) - L(t_{ref})}{L(t_{ref})}\right) \cdot 10^6\ \mu m/m \qquad (2)$$

in which L(t) [mm] is the length of solely the concrete element inside the mould at time t, t_{ref} [s] is the reference time at which the autogenous shrinkage is zeroed out and t [s] is the time instant. As in case of 3D printing, the first 24h are of highest importance, only these results are represented within this paper. Shrinkage graphs are zeroed out at the knee-point t_{kn} [s], which represents the final setting time and is measured by performing automated VICAT measurements for every mix composition.

2.4. Mercury Intrusion Porosimetry (MIP)

The occurrence of capillary pores, with a diameter between 10nm and 10µm, was studied based on Mercury Intrusion Porosimetry (MIP) measurements (PASCAL series 140 and 440, Thermo Fisher Scientific Inc.). For these measurements, cylinders with a diameter of 14 mm were drilled out of a double-layered filament (Figure 1(a)) and freeze-dried at an age of 28 days for 7 days after being put in liquid nitrogen. Afterwards, these cylinders were cut into three equal parts to make a distinction between the porosity of the upper, lower and interlayer zone (Figure 1(b)).

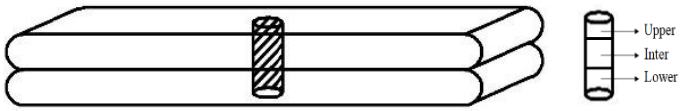

(a) (b)

Figure 1 : (a) Cylindrical specimens (Ø = 14 mm), drilled out a double-layered specimen and (b) indication of the different zones investigated during MIP measurements

2.5. Air void analysis

The air content of hardened double-layered specimens was analysed according to the linear traverse method as described by ASTM C457 by means of a fully automated concrete Experts International RapidAir 457 device. The printed specimens were longitudinally sawn in half (Figure 2) at an age of 28 days and both sides were polished with variable grading. After polishing, the samples were dried for one hour at 35°C and treated with black ink and barium sulphate ($BaSO_4$) to increase the contrast between the air voids and the cement matrix. After scanning the complete surface, the RapidAir 457 device provides the air content A [vol%] based on the number of voids intersected during the scanning procedure T_a [mm] divided by the total chord length T_{tot} [mm] which is according to ASTM C457 equal to 2413mm.

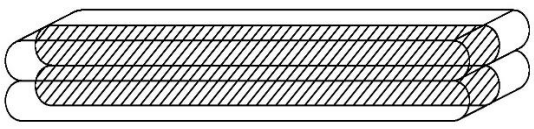

Figure 2: Longitudinal specimens used for air void analysis

3. RESULTS

3.1. Shrinkage

Figure 3 and Figure 4 represent, respectively, the autogenous shrinkage and unprotected shrinkage of the mixtures with and without superabsorbent polymers. Both graphs depict the same trend: in case of a reference mixture shrinkage starts immediately after final setting, while mixtures including SAPs show at first instance a swelling behaviour for approximately 24h. The expansive character of SAP addition is ascribed to the combination of their water mitigation capacity and a chemical swelling present in all mixtures. However, in case of the reference mixture this chemical swelling is not enough to overcome the omnipresent capillary tension. After final setting, the chemical-structural swelling can occur due to the relatively late formation and growth of calcium hydroxide. This will create a crystallisation pressure that counteracts the capillary pore water tension that induces self-desiccation. In case of samples with SAPs, the solid matrix is believed to be more elastic as there is still water supplied to unhydrated cement particles and as such the structuration continues more actively compared to the reference material. Also, the fresh CSH rims that are formed around these unhydrated particles surrounded by water, are larger in volume then their unhydrated counterparts [7].

Once hydration slows down as it reaches its optimum, all mixtures can only shrink under endured evaporation. Comparing the different SAPs, one can also conclude that the swelling behaviour of SAP A lasts longer compared to SAP P and this behaviour can be attributed to the more gradual release of entrapped water while SAP P will release the stored water more quickly [3].

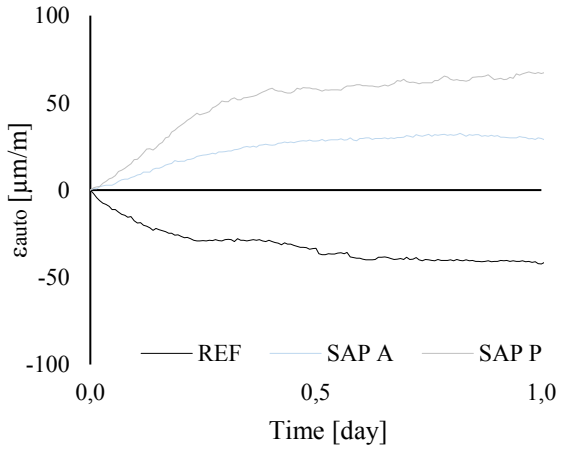

Figure 3: Autogenous shrinkage zeroed out at t_{kn}

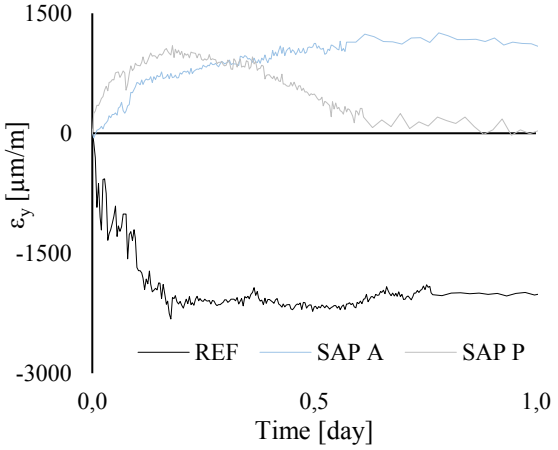

Figure 4: Unprotected shrinkage zeroed out at t_{kn}

3.2. Pore size and pore size distribution

Mercury intrusion porosimetry measurements led to the findings in Table 3 and Figure 4. In general, mixtures with SAPs tend to increase the total nanoporosity in all the layers of the hardened specimens. This confirms with the conclusion stated by Baroghel-Bouny [7]: when the (total) w/c ratio decreases, the nanoporosity decreases as well. This is associated to the denser matrix that results from a reduction in total amount of mixing water.

No conclusive statement can be made about which zone (i.e. upper, inter or lower) has the largest nanoporosity, however there is a clear difference in continuous pore network as

suggested by the distinct variations in derivative intrusion curves (Figure 4). From the median diameters, it is concluded that in general, the bottom layer has the network with the smallest continuous pore diameter. This is ascribed to the densification under additional hydrostatic pressure, exerted by the top layer.

In general, SAPs tend to reduce the amount of nanopores in the range of 100 nm to 500 nm and increase the amount of voids with a diameter above 700 nm. This is ascribed to a better hydration rate around the SAPs, closing up the smaller pores, as well as to their autogenous shrinkage mitigation that reduces the amount of micro cracking [3]. This phenomenon will reduce the amount of ingress paths for chemical substances and result in a more durable material behaviour compared to the reference mix composition.

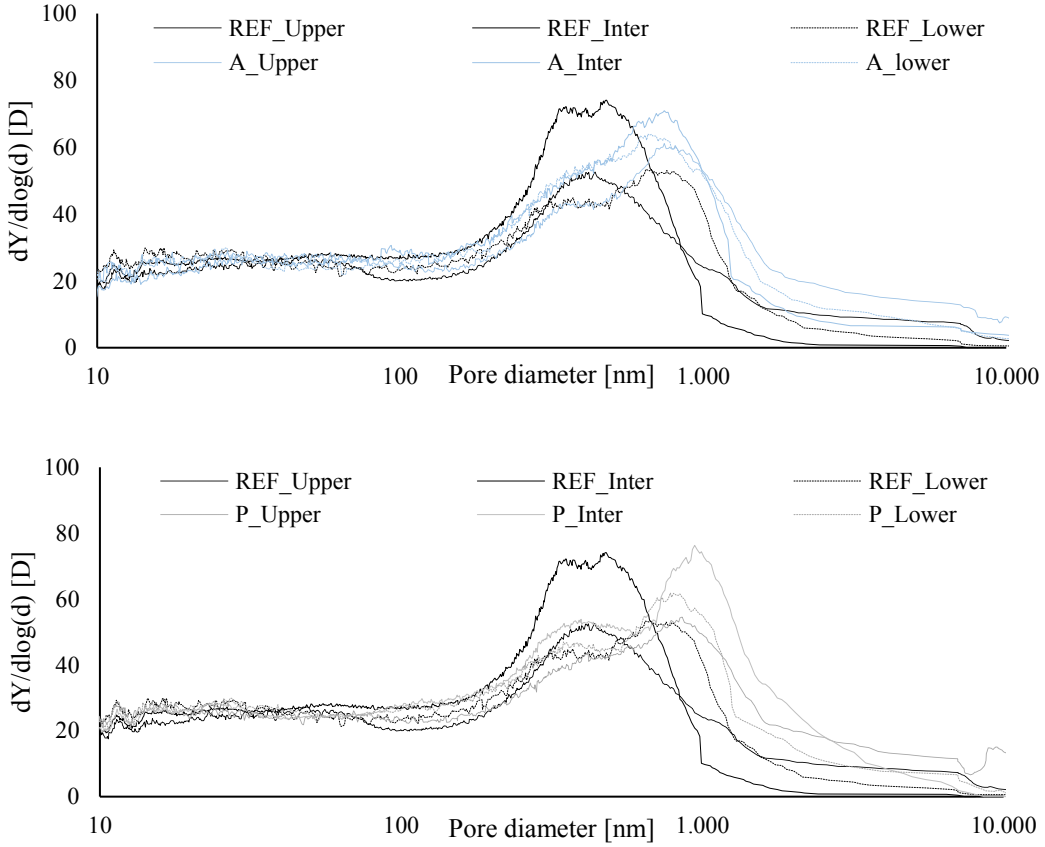

Figure 5 : Derivative intrusion curves obtained for mixtures with and without SAPs

Table 3: Nanoporosity

Sample	Total porosity <10 µm [%]				Median diameter [nm]		
	Upper	Inter	Lower	Overall	Upper	Inter	Lower
REF	15.2	16.2	15.9	16.2	255.6	273.2	246.6
SAP A	19.1	18.4	18.4	18.6	384.4	336.1	327.5
SAP P	17.4	19.9	17.6	18.3	355.1	388.3	299.4

3.3. Air void analysis

Figure 5 depicts the cumulative air content obtained by the RapidAir test. The total air content increases with SAP addition and the exact increase is more or less proportional to the amount of SAPs added. The expected size of the resulting macro pores based on the SAP initial size and absorption capacity of mixing water is 426 ± 94 µm and 846 ± 272 µm for SAP A and SAP P, respectively. This is exactly the range as found by RapidAir measurements. Based on a visual inspection of the studied specimens (Figure 6), one can also conclude that the printing process has no influence on the air void distribution within the sample and there is no clear distinction of the interlayer visible. This is already proven in previous research [8] and the results are similar for mixtures including SAPs. The latter research also mentioned the entrapment of air voids at the interlayer in case of increased time gaps. However, as the addition of SAPs increases the moisture content of the surface, further research on the air void distribution in case of different time gaps is required. The higher amount of voids can also affect the mechanical properties (i.e. compressive strength and interlayer bonding strength), but these investigations are not within the scope of this research.

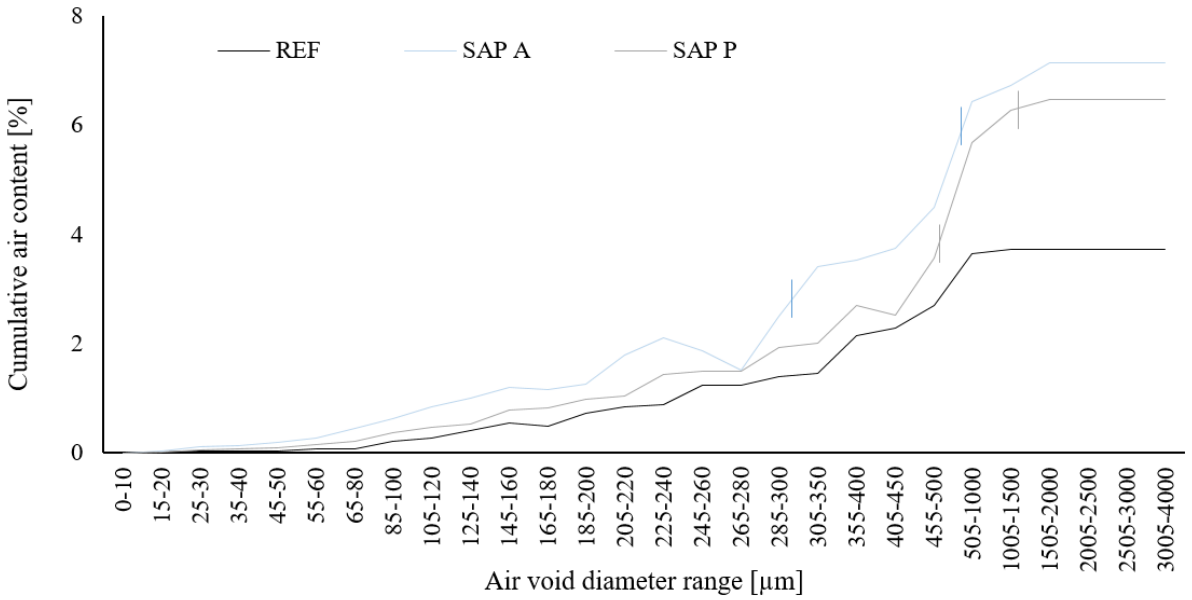

Figure 6: Cumulative air content in hardened specimens

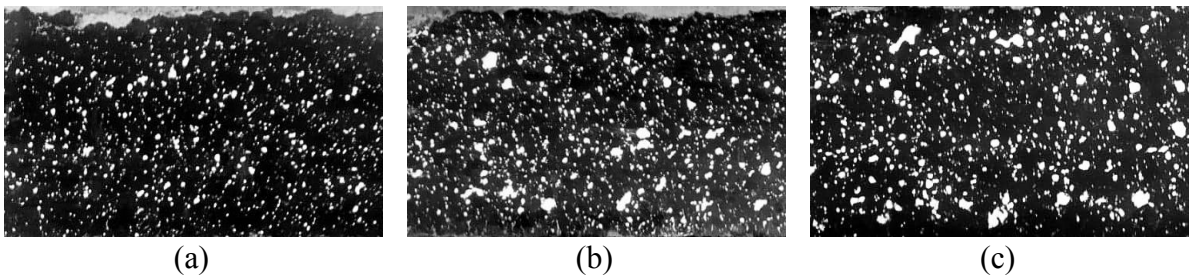

(a) (b) (c)

Figure 7: Studied specimens in RapidAir test : (a) Reference composition, (b) mixtures containing SAP A, (c) mixtures containing SAP P

4. CONCLUSIONS

The effect of two different types of SAPs on the shrinkage behaviour and microstructure of a 3D printed cementitious element is investigated and the following conclusions can be drawn:

- Superabsorbent polymers reduce shrinkage due to internal curing. SAP A shows better properties due a more gradual release of entrained water;
- Both SAPs decrease the nanoporosity in the range of 100 nm to 500 nm. This is ascribed to a better hydration rate around the SAPs, closing up the smaller pores, as well as to their autogenous shrinkage mitigation that reduces the amount of micro cracking resulting in a lower amount of preferential ingress paths for chemical substances;
- The porosity of the different zones within a printed specimen is comparable for all mixture compositions;
- The total air content increase with SAP addition and the exact increase is proportional to the amount of SAPs added.

ACKNOWLEDGEMENTS

J. Van Der Putten would like to acknowledge the support by EFRO for the C3PO-project (B/15100/01). D. Snoeck is a postdoctoral fellow of the Research Foundation-Flanders (FWO) and would gratefully acknowledge for the financial support of project No.12J3620N.

REFERENCES

1. De Schutter, G., et al., *Vision of 3D printing with concrete — Technical, economic and environmental potentials.* Cement and Concrete Research, 2018. **112**: p. 25-36.
2. Bos, F., et al., *Additive manufacturing of concrete in construction: potentials and challenges of 3D concrete printing.* Virtual and Physical Prototyping, 2016. **11**(3): p. 209-225.
3. Snoeck, D., *Self-healing and microstructure of cementitious materials with microfibres and superabsorbent polymers*, in *Faculty of Engingeering and Architecture* 2015, Ghent University.
4. Mechtcherine, V., et al., *Effect of internal curing by using superabsorbent polymers (SAP) on autogenous shrinkage and other properties of a high-performance fine-grained concrete: results of a RILEM round-robin test.* Materials and Structures, 2014. **47**(3): p. 541-562.
5. Mejlhede Jensen, O. and P. Freiesleben Hansen, *Water-entrained cement-based materials: I. Principles and theoretical background*. Vol. 31. 2001. 647-654.
6. Snoeck, D., C. Schröfl, and V. Mechtcherine, *Recommendation of RILEM TC 260-RSC: testing sorption by superabsorbent polymers (SAP) prior to implementation in cement-based materials.* Materials and Structures, 2018. **51**(5): p. 116.
7. Baroghel-Bouny, V., et al., *Autogenous deformations of cement pastes: Part II. W/C effects, micro–macro correlations, and threshold values.* Cement and Concrete Research, 2006. **36**(1): p. 123-136.
8. Van Der Putten, J., et al., *Microstructural Characterization of 3D Printed Cementitious Materials.* Materials, 2019. **12**(18).